Research Article

Synthesis, Characterization, and Comparison of Pure Zinc Oxide and Magnesium-Doped Zinc Oxide Nanoparticles and their Application on Ethanol Sensing Activities

N. Kangathara [iD],[1] **V. Sabari** [iD],[2] **L. Saravanan** [iD],[1] **and S. Elangovan** [iD][3]

[1]*Department of Physics, Saveetha School of Engineering, Saveetha Institute of Medical and Technical Sciences, Thandalam, Chennai 602 105, India*
[2]*Department of Physics, Marudhar Kesari Jain College for Women, Vaniyambadi, India*
[3]*Department of Physics, College of Natural and Computational Sciences, Wollega University, Ethiopia 395*

Correspondence should be addressed to S. Elangovan; elangovan.physics@rediffmail.com

In this study, we reported the synthesis of pure ZnO and Mg-doped ZnO (Mg-ZnO) nanoparticles by simple co-precipitation method and studied the ethanol sensing activity of the synthesized nanostructures. XRD analysis illustrates that the synthesized ZnO and Mg-doped ZnO nanoparticles (NPs) possess hexagonal wurtzite structure and the average crystallite size is calculated to be 29 nm and 33 nm, respectively. The FT-IR spectra of pure and Mg-doped ZnO NPs confirm that the presence of bands appeared near 400 cm^{-1} for Zn-O and the bands at 622 cm^{-1} can be attributed to Mg-O stretching modes. The band gap energy estimated from the absorption spectra for ZnO and Mg-ZnO NPs, respectively, at 3.26 eV and 3.32 eV, displays the considerable optical property. Further, we observed that the UV-Vis spectroscopic data exhibits high absorbance in the UV range for the prepared samples. The SEM images clearly display the needle-like morphology of the synthesized samples. Dynamic light scattering analysis shows average particle size of 110 nm. The ethanol sensing measurements were carried out with 100 ppm concentration, and the linear responses from ZnO and Mg-ZnO NPs-based sensors are detected in the working temperature of 350°C. The obtained results demonstrated that the synthesized Mg-ZnO nanostructures have improved conductivity with larger active surface area for the most promising application in the ethanol sensing activity.

1. Introduction

Semiconducting metal oxide nanostructures are having a very large surface-to-volume ratio, and the gas-sensing properties strongly depend on a specific surface area. Nanostructure-based gas sensors made from these semiconducting metal oxides are projected to establish significant sensing properties. Further the properties of nanomaterials can be tailored without modifying the chemical composition [1] and having unique quantum effect [2]. The quantization energy modifies the band structure of nanomaterials and makes it promising with altered magnetic, optical, and electronic properties for various applications [3, 4]. Nanomaterials have acquired greater attention by researchers due to their unique properties and applications in the field of opti-

cal, medicine, and ecology [5]. Nowadays, the metal or metal oxide nanoparticles synthesized with smaller sizes and shapes are in high demand due to their size and unique optical properties such as surface plasmon resonance [3]. Notably, the ZnO nanostructure-based gas sensors have caught huge consideration. The wurtzite structure of ZnO nanoparticles has a large surface area, large band gap, and high excitation energy which makes it a suitable material for sensor applications [6].

The zinc oxide nanoparticles are nontoxic and biocompatible, and it can be produced with low cost. Chin Boon Ong et al. in 2018 [7] and several researchers have done a review on how ZnO nanoparticles have been used as a photocatalyst and for other environmental applications [8]. Prabhakar Rai et al. reported the hydrothermal synthesis of

ZnO nanoparticles assisted with trisodium citrate. It was shown that ZnO NPs-based gas sensors can be used for sensing NO_2 at low temperature and the acetaldehyde can be sensed at high temperature [9]. Erol et al. has synthesized ZnO nanoparticles using sol gel method and reported that the ZnO nanoparticles are found as a potential material to be used for the fabrication of high-sensitive humid sensors [10]. Ikram and his co-workers demonstrated the construction of hybrid organic solar cells by mixing ZnO and TiO_2 nanoparticles to the active layer of photovoltaic devices [11]. The doped ZnO nanostructure has proven applications in many fields such as sensing, biomedicine, and photocatalyst [7, 12]. Pascariu et al. have synthesized a Ni, Co-doped ZnO nanoparticles by simple co-precipitation method and investigated the degradation of Rhodamine B with pure and doped samples [13]. Recently Zhang et al. described the preparation of Au/ZnO NPs and conducted the low-temperature sensing activity with 100 ppm CH_4 concentration [14]. Controlling the performance of gas sensing could be achieved by manipulating the concentration of charge carriers and defects [15]. Additionally, the conductivity of ZnO NPs can also be tuned by varying the doping level or changing the morphology [16, 17].

Magnesium oxide (MgO) has a larger band gap of 7.8 eV; hence, it is a perfect material to incorporate into ZnO to widen the band gap by varying the Mg content, which are considered to be most suitable for photocatalytic applications [18]. Doping Mg with ZnO will increase the conduction electrons, thus increasing the conductivity in ZnO [19]. Wang et al. [20] have synthesized the Mg-doped ZnO nanoparticles by auto combustion method and proved that ZnO with optimal Mg content enhances the photocatalytic activity. The nanoparticles of pure and Mg-doped ZnO were synthesized by sol-gel method, and its sensing ability was investigated by Jaballah et al. in 2020 [21]. It was reported that Mg-doped ZnO thin film sensor at room temperature has shown a higher response of 796 toward 100 ppm of ammonia gas [22].

The ethanol sensing measurements have gained a huge attention in the field of food, biological industries, and environmental applications [23]. It has serious effects on profuse usage and is also shown to cause organ failure, depression, and personality disorder. A high level of ethanol content is found in alcohol, and the consumption is prohibited while driving. The ethanol breath test is one such method used to monitor and to reduce alcohol consumption while driving. This paves a way of interest in the development of sensors for accurate and instant detection of ethanol vapor for public health and environmental safety [24]. But there were some limitations on the detection of ethanol at very low concentration. In this context, Arakawa et al. [25] have successfully constructed a biosniffer, a highly sensitive biochemical gas sensor in order to find the concentration of ethanol on human skin. It can measure ethanol gas in a concentration range of 25 ppb–128 ppm. Liu et al. [26] designed a gas sensor with ZnO/SnO_2 composite for highly sensitive ethanol detection having concentration of 100 ppm in the working temperature of 225°C. Earlier it was also reported that the gas sensing response of the MoO_3 sample toward 100 ppm

of ethanol vapor is 59% at 350°C [27]. In this paper, we report the inexpensive way of synthesizing the pure ZnO and magnesium-doped ZnO NPs (Mg-ZnO) by simple co-precipitation method, and the physical properties of synthesized NPs were studied by powder X-ray diffraction (XRD), Fourier transform infrared spectra (FTIR), UV-visible spectroscopy, and scanning electron microscopy (SEM), and the particle size distribution was measured by dynamic light scattering (DLS). We attempt to demonstrate the low concentration ethanol sensing behavior of these synthesized ZnO and Mg-ZnO nanoparticles at higher working temperature.

2. Experimental

2.1. Materials. Zinc sulfate [$ZnSO_4.7H_2O$], magnesium nitrate [$Mg[NO_3]_2$], and sodium hydroxide [NaOH] are used for the synthesis of ZnO and Mg-doped ZnO nanoparticles. All the chemicals used in this experiment were purchased from Sigma-Aldrich, India.

2.2. Synthesis of Pure ZnO. 9.1016 g of zinc sulfate [$ZnSO_4.7H_2O$] is dissolved in 200 ml doubly deionized water to get an aqueous solution [0.1 M] which is used as the host precursor. After stirring the aqueous solution for one hour, the NaOH pellets were slowly added until the pH value was adjusted to 9 and milky solution was obtained. Then, the mixture was heated up to 80°C and stirred continuously for 2 hours. Allow the solution to keep at rest for 1 hour to get precipitation. The precipitate is then filtered and washed with ethanol and water of ratio 1 : 3 and allows it to dry. The collected ZnO sample was then dried in a microwave oven at temperature of 100°C for 2 hours and grounded using mortar to make fine powder of ZnO particles. Finally, the obtained ZnO nanoparticles were annealed at 500°C for 2 hours. The graphical abstract to represent the synthesis procedure is shown in Figure 1.

2.3. Synthesis of Mg-Doped ZnO NPs. To synthesize Mg-doped ZnO nanoparticles, the above discussed method was followed. Typically, the aqueous solution of 0.1 M is prepared by mixing 9.1016 g of zinc sulfate [$ZnSO_4.7H_2O$] in 200 ml of distilled water. Then, add 0.09987 g of magnesium nitrate into the host precursor solution under continuous stirring. After one hour, the NaOH pellets were slowly added until the pH value was adjusted to 9 and milky solution was obtained. Then, the mixture was heated up to 80°C and stirred continuously for 2 hours. Allow the solution to keep at rest for 1 hour to get precipitation. The precipitate is then filtered and washed with ethanol and water of ratio 1 : 3 and allows it to dry. The collected ZnO sample was then dried in an oven at temperature of 100°C for 2 hours and grounded using mortar to make fine powder of Mg-ZnO particles. Finally, the obtained Mg-doped ZnO nanoparticles were annealed at 500°C for 2 hours. The flow chart in Figure 2 represents the synthesis procedure of Mg-doped ZnO (Mg-ZnO) NPs.
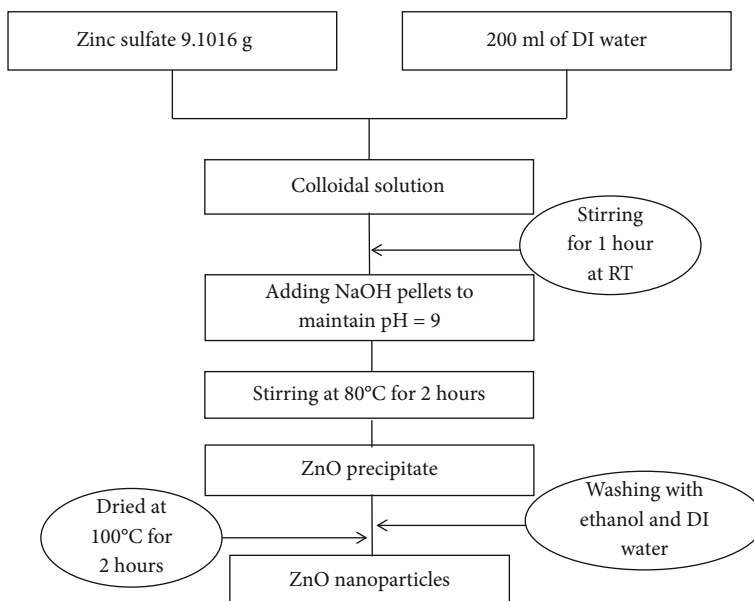
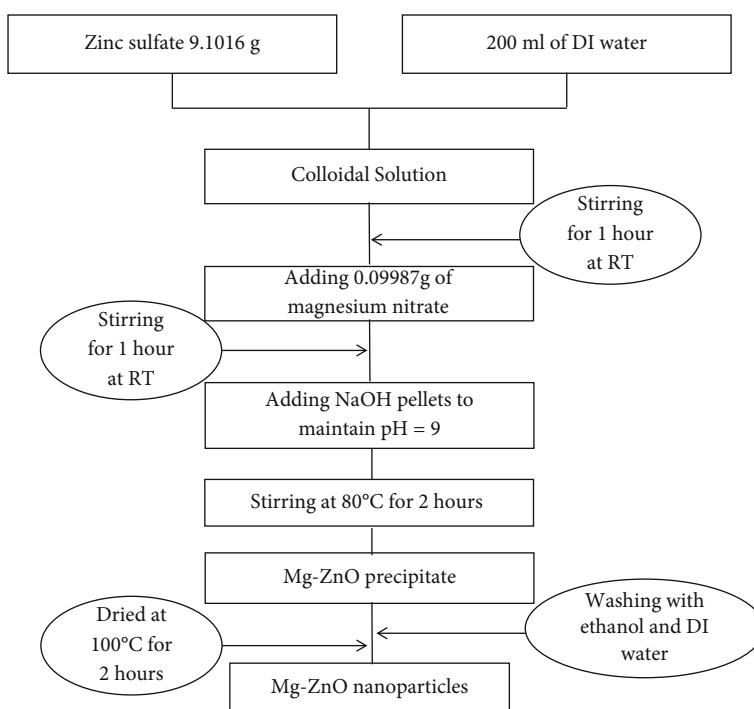FIGURE 1: Synthesis scheme of ZnO nanoparticles by co-precipitation method.

FIGURE 2: Flow chart for the synthesis of Mg-doped zinc oxide nanoparticles.

3. Results and Discussion

3.1. Structural Analysis of Pure ZnO and Mg-Doped ZnO Nanoparticles. Figure 3 shows the XRD pattern of the synthesized pure ZnO and Mg-ZnO nanoparticles. The observed diffraction peaks from the XRD pattern for both the ZnO and Mg-doped ZnO nanoparticles agreed well with the hexagonal structure of ZnO oxide with JCPDS card no 36-1451 [28], and the particles are high crystalline in nature.

The major peaks located at the angle of 2θ =31.70, 34.35, and 36.2° correspond to (100), (002), and (101) planes of the ZnO. There is no such additional peak observed for the magnesium metal. The average crystalline size has been approximately 29 and 33 nm, respectively, for ZnO and Mg-ZnO, and the obtained line broadening is only due to small crystalline size. The size of the crystallite can be calculated from the Debye Scherer's formula given in the Equation (1). Compared to the pure ZnO, it can be seen in XRD pattern that
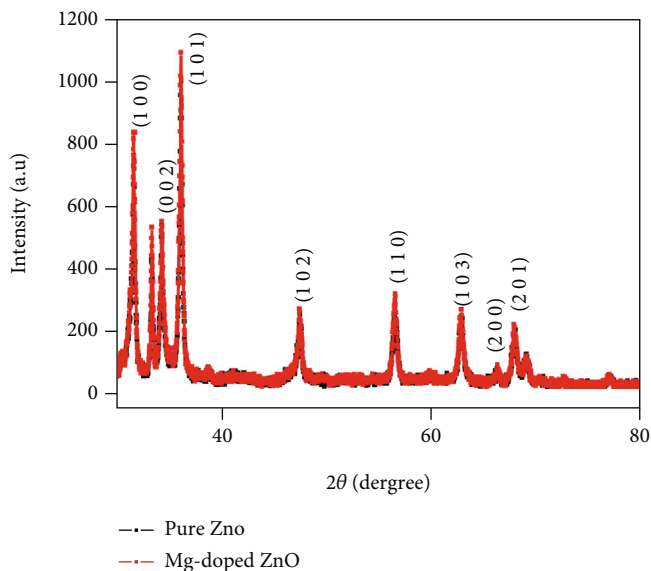
FIGURE 3: XRD pattern of pure and Mg-doped ZnO nanoparticles.

the Mg doping in ZnO leads to an increase in the intensity of the (101) diffraction peak at the angle of 36.20°.

$$D = \frac{K\lambda}{\beta Cos\theta}, \tag{1}$$

where D is the average crystallite size, θ is the Bragg's angle, λ is the wavelength of the X-ray beam, β is the full width at half maximum of the diffraction peaks, and K is a constant approximately equal to 0.9 [29].

3.2. Vibrational Analysis. The FT-IR spectra of pure ZnO and Mg-doped ZnO oxide nanoparticles are shown in Figure 4. FTIR analysis is a suitable technique to evaluate the functional groups present in the samples subjected to analysis [30]. The samples shown the bands appeared approximately near $400\,cm^{-1}$ for Zn-O [31] and the wider band at 320, and a sharp band at $622\,cm^{-1}$ can be attributed to Mg-O stretching modes. Oxides and hydroxides of metal nanoparticles generally give an absorption peak in the fingerprint region, i.e., below wavelength of $1000\,nm$ arising from the interatomic vibrations [32]. The absorption bands at 1634 and $1636\,cm^{-1}$ in the spectra for ZnO and Mg-ZnO can be attributed to C=C stretching vibrations. The weak intensity peaks originated around $2800\text{-}2900\,cm^{-1}$ are due to C–H bonds, for both the samples. The wide absorption bands appeared at 3507 and $3514\,cm^{-1}$ for pure ZnO and Mg-ZnO are attributed stretching vibration mode of a hydroxyl (O=H) group [33] and Zn–OH and Mg–Zn–OH. There is a considerable peak shift of Zn-O band which can be a secondary evidence of Mg content in the lattice. The above result indicates that the synthesized ZnO nanoparticle is doped with magnesium [34].

3.3. Optical Analysis. The optical characterization of the samples was recorded on the UV-Vis absorption spectrum, and the data were recorded between 200 and 1200 nm.
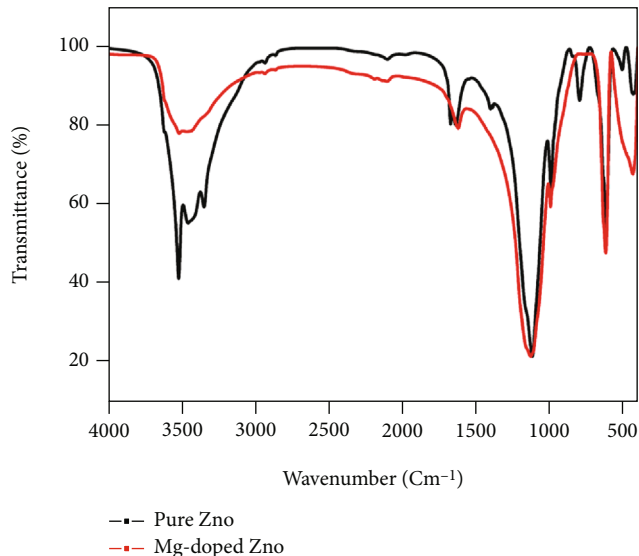

FIGURE 4: FT-IR vibrational spectra of pure ZnO and Mg-doped ZnO.

Figure 5 shows the UV-Vis spectrum of pure ZnO and Mg-doped ZnO NPs. The absorption takes place in the regions of entire visible region. The absence of additional absorption peaks confirms that the synthesized samples have significant optical properties. From the Figure 5, the absorption edge for pure ZnO is at a wavelength of 380 nm. From the UV absorption spectra, the higher cut-off wavelength of Mg-doped ZnO lies near 375 nm. The band gap of all the samples can be estimated by converting wave length into the energy using the following equation, where E is the band gap energy, h is Planck's constant, c is the velocity of light, and λ is the maximum wave length.

$$E = \frac{hc}{\lambda}. \tag{2}$$

The band gap of pure ZnO is calculated by observing the maximum absorption peak from the UV-Vis spectra and found to be 3.26 eV, and for Mg-doped ZnO, it is found to be increased with the value of 3.32 eV. Due to the Mg doping, there was a slight shift observed toward the lower wavelength. Further noted that the absorption intensity at the UV region increases for Mg-ZnO nanoparticles, and this might be due to increase in the charge carrier concentration [35]. Hence, it is confirmed that while doping with Mg, the band gap of ZnO is increased, and the conductivity is also increased.

3.4. Dynamic Light Scattering [DLS] Analysis. DLS technique is used to measure the distribution of particles in colloidal solutions. It is also used to measure the Zeta potential, molecular weight, and concentration of nanoparticles [36]. Figure 6 exhibits the distribution of particle size for pure ZnO and Mg-doped ZnO nanoparticles and the particle distribution starting from 40 to 600 nm with the maximum size distribution around 110 nm with the polydispersity index (P.I.) of 0.301 for Mg-ZnO. Pure ZnO sample with broad
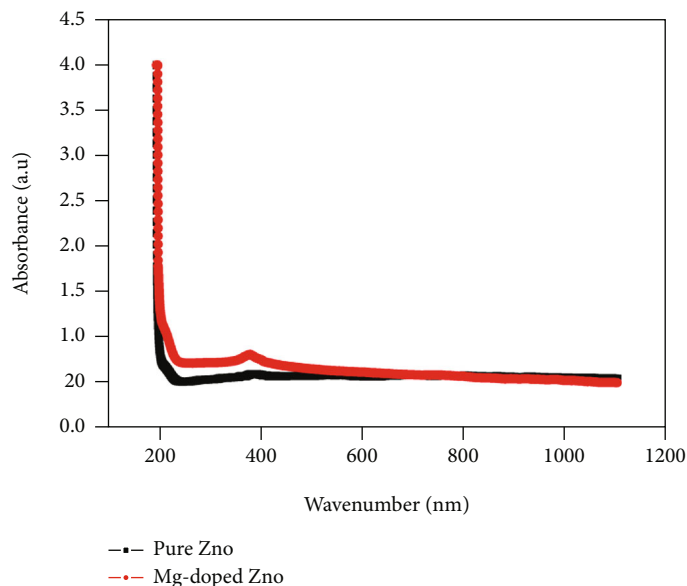
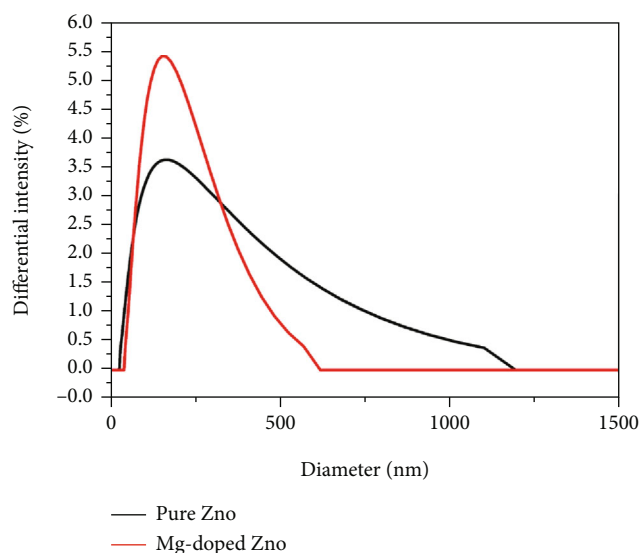FIGURE 5: UV-Vis spectra of pure ZnO and Mg-doped ZnO nanoparticles.

FIGURE 6: DLS spectra for pure and Mg-doped ZnO.

size distribution (P.I. = 0.315) indicates the moderate distribution of ZnO nanoparticles in the solvent.

3.5. Morphological Analysis. The surface morphology of synthesized nanoparticles is studied by scanning electron microscope (SEM). Figures 7(a) and 7(b) show the SEM images of pure and Mg-doped ZnO nanostructures. The SEM image of pure ZnO nanoparticles has partial needle shape and tetragonal shapes with sizes smaller than 1 micrometer in length. It is seen that the structure of the particles is due to the agglomeration of the particles. This aggregation of particles might have arises from the high surface energy of the synthesized nanoparticles [37]. But some of the particles appear to have regular shape and uniformly distributed which are due to the better solubility of the reactant with the solvent.

3.6. Ethanol Sensing. Figure 8 displays the responses of ZnO and Mg-ZnO-based sensors, as a function of time at the optimal working temperature of 300°C. As shown in the figure, the sensor resistance significantly decreased for increase in the Mg doping concentration from 1% to 5% in ZnO during the exposure of 100 ppm of ethanol, in accordance to the general sensing mechanism of n-type oxide semiconductors. In fact, the gas detection mechanism relies on a variation in electrical conductivity or resistance due to gas adsorption and desorption on the sensor surface. The resistance curve of the sensor in Figure 8 displayed the recovery time of 30 s, for 100 ppm of ethanol gas at the working temperature of 300°C. The smaller crystallites provide much larger effective surface area to react with the gas and induce the positive effect on sensitivity. It was previously stated that the metal ion doping could tune the band gap by influencing the surface potential and increase the carrier concentration in the host material [38]. The inclusion of Mg into the ZnO structure enhances the sensing mechanism due to the lattice disorder hosted by the Mg^{2+} ions, and large numbers of reactive oxygen molecules are adsorbed on the surface and available to interact with the reductive gases, and hence, the conductivity of the material gets increased [39]. This type of Mg-doped ZnO-based sensor has a great potential for sensing toxic (reducing gases) ethanol gas, and it shows a notable response at high temperature around 300°C. The gas sensing tests indicate that the Mg-ZnO presents higher conductivity than pristine ZnO. This result supports the increment in the density of the free charge carriers upon doping.

3.7. Conclusion. The pure ZnO and Mg-doped ZnO nanoparticles have been successfully synthesized by simple co-precipitation method. XRD analysis confirmed the formation of ZnO and Mg-ZnO NPs with hexagonal structure, and the average crystallite size calculated is 29 nm and

(a)   (b)
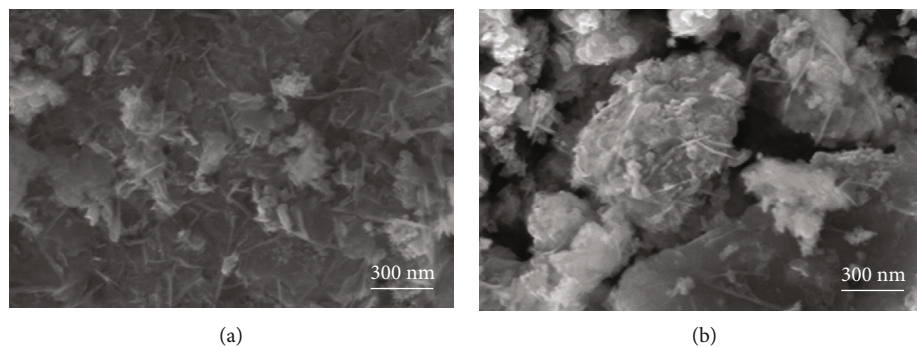
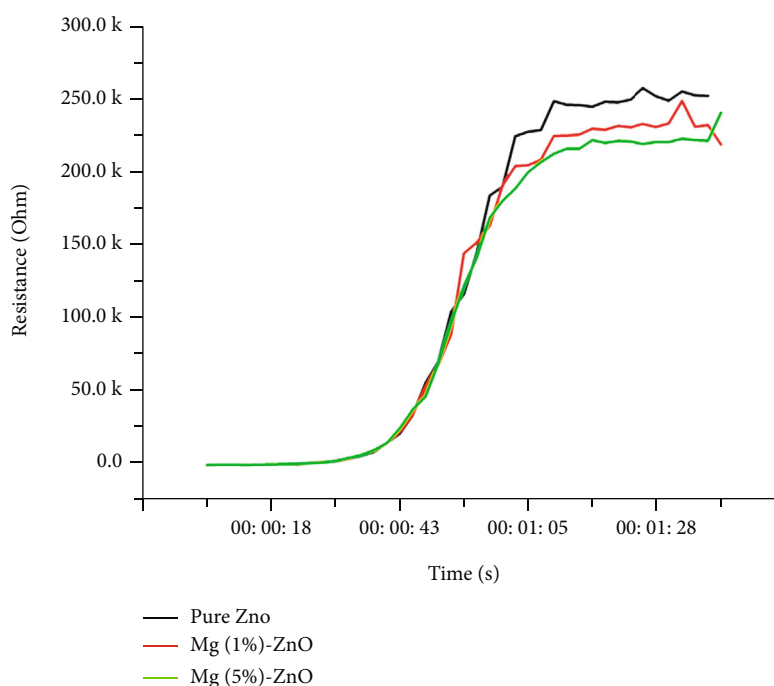FIGURE 7: SEM analysis of (a) pure ZnO and (b) Mg-doped ZnO.

FIGURE 8: Ethanol sensing characteristic curves of pure ZnO and Mg-doped ZnO.

33 nm, respectively. The FTIR analysis confirms the presence of standard stretching of O=H and the strong C=C stretching modes for both pure and Mg-doped ZnO NPs. The peaks appeared below $400\,cm^{-1}$ confirm the presence of Zn-O and Mg-O molecular vibrations. UV-Vis absorption spectrum illustrates that the band gap is 3.26 eV for ZnO and 3.32 eV for Mg-ZnO and confirms the shift in the spectra due to Mg doping. SEM clearly shows that the average size of particles is in the range of nanometer and has a needle-like structure with partial agglomeration. The particle size distribution of ZnO and Mg-doped ZnO using the DLS technique revealed that the particle size of 110 nm and the polydispersity index of 0.301 were found, indicating the uniform size distribution of nanoparticles. The ethanol sensing measurement was observed for the samples, and the results reveal that the 5% Mg-doped ZnO demonstrates higher conductivity than pristine ZnO and it shows an enhanced performance in ethanol gas sensing and used as a prominent candidate for gas sensing applications.

Data Availability

The data will be available made on reasonable request. The data set on which this paper is in Excel format, i.e., all the calculations are done in Excel, and graphs are drawn in Origin software.

Ethical Approval

This work does not involve human participants and/or animals.

Conflicts of Interest

The authors declared no potential conflicts of interest.

Authors' Contributions

N. Kanagathara has contributed to the methodology, conceptualization, and writing–original draft. V. Sabari has

contributed to the data curation, validation, and visualization. L. Saravanan has contributed to the critical revision. S. Elangovan has contributed to the supervision, formal analysis, review, and editing.

Supplementary Materials

The spectral data of this work has been uploaded in the supplementary file. This file consists of XRD, FTIR, DLS, and sensing experimental data related with the various parameters as plotted in the manuscript. *(Supplementary Materials)*

References

[1] D. L. Leslie-Pelecky and R. D. Rieke, "Magnetic properties of nanostructured materials," *Chemistry of Materials*, vol. 8, no. 8, pp. 1770–1783, 1996.

[2] W. Y. Li, L. N. Xu, and J. Chen, "Co_3O_4 nano materials in lithium-ion batteries and gas sensors," *Advanced Functional Materials*, vol. 15, no. 5, pp. 851–857, 2005.

[3] K. K. Nanda, S. N. Sahu, and S. N. Behera, "Liquid drop model for the size-dependent melting of low-dimensional systems," *Physical Review A*, vol. 66, no. 1, p. 013208, 2002.

[4] M. Ikram, R. Tabassum, U. Qumar et al., "Promising performance of chemically exfoliated Zr-doped MoS2 nanosheets for catalytic and antibacterial applications," *RSC Advances*, vol. 10, no. 35, pp. 20559–20571, 2020.

[5] M. Ikram, A. Raza, M. Imran, A. Ul-Hamid, A. Shahbaz, and S. Ali, "Hydrothermal synthesis of silver decorated reduced graphene oxide (rGO) nanoflakes with effective photocatalytic activity for wastewater treatment," *Nanoscale Research Letters*, vol. 15, no. 1, pp. 1–11, 2020.

[6] N. P. Shetti, S. J. Malode, D. S. Nayak et al., "Fabrication of ZnO nanoparticles modified sensor for electrochemical oxidation of methdilazine," *Applied Surface Science*, vol. 496, pp. 143656–143658, 2019.

[7] C. B. Ong, L. Y. Ng, and A. W. Mohammad, "A review of ZnO nanoparticles as solar photocatalysts: synthesis, mechanisms and applications," *Renewable and Sustainable Energy Reviews*, vol. 81, no. 1, pp. 536–551, 2018.

[8] M. Ali, M. Ikram, M. Ijaz, A. Ul-Hamid, M. Avais, and A. A. Anjum, "Green synthesis and evaluation of n-type ZnO nanoparticles doped with plant extract for use as alternative antibacterials," *Applied Nanoscience*, vol. 10, no. 10, pp. 3787–3803, 2020.

[9] P. Rai and Y.-T. Yul, "Citrate-assisted hydrothermal synthesis of single crystalline ZnO nanoparticles for gas sensor application," *Sensors and Actuators B: Chemical*, vol. 173, pp. 58–65, 2012.

[10] A. Erol, S. Okur, B. Comba, Ö. Mermer, and M. Ç. Arıkan, "Humidity sensing properties of ZnO nanoparticles synthesized by sol–gel process," *Sensors and Actuators B: Chemical*, vol. 145, no. 1, pp. 174–180, 2010.

[11] M. Ikram, R. Murray, M. Imran, S. Ali, and S. Ismat Shah, "Enhanced performance of P3HT/(PCBM: ZnO:TiO2) blend based hybrid organic solar cells," *Materials Research Bulletin*, vol. 75, pp. 35–40, 2016.

[12] M. Rashid, M. Ikram, A. Haider et al., "Photocatalytic, dye degradation, and bactericidal behavior of Cu-doped ZnO nanorods and their molecular docking analysis," *Dalton Transactions*, vol. 49, pp. 8314–8330, 2020.

[13] P. Pascariu, I. V. Tudose, M. Suchea, K. Emmanouel, N. Fifere, and A. Airinei, "Preparation and characterization of Ni, Co doped ZnO nanoparticles for photocatalytic applications," *Applied Surface Science*, vol. 448, no. 1, pp. 481–488, 2018.

[14] B. Zhang, Y. Wang, X. Meng, Z. Zhang, and S. Mu, "High response methane sensor based on Au-modified hierarchical porous nanosheets-assembled ZnO microspheres," *Materials Chemistry and Physics*, vol. 250, p. 123027, 2020.

[15] T. Shujah, M. Ikram, A. R. Butt et al., "Growth of zinc oxide and zinc stannate nanostructured thin films for carbon monoxide sensing application," *Nanoscience and Nanotechnology Letters*, vol. 11, no. 8, pp. 1050–1059, 2019.

[16] J. Xu, S. Li, L. L. Li, L. Chen, and Y. Zhu, "Facile fabrication and superior gas sensing properties of spongelike Co-doped ZnO microspheres for ethanol sensors," *Ceramics International*, vol. 44, no. 14, pp. 16773–16780, 2018.

[17] N. J. Ridha, H. B. A. Kadhim, F. K. M. Alosfur, and R. T. Ahmed, "ZnO nanofluids prepared by laser ablation in various solvents," *Materials Research Express*, vol. 5, no. 12, p. 125008, 2018.

[18] V. Etacheri, R. Roshan, and V. Kumar, "Mg-doped ZnO nanoparticles for efficient sunlight-driven photocatalysis," *ACS Applied Materials & Interfaces*, vol. 4, no. 5, pp. 2717–2725, 2012.

[19] V. K. Samoei and A. H. Jayatissa, "Aluminum doped zinc oxide (AZO)-based pressure sensor," *Sensors and Actuators A: Physical*, vol. 303, p. 111816, 2020.

[20] Y. Wang, X. Zhao, L. Duan et al., "Structure, luminescence and photocatalytic activity of Mg-doped ZnO nanoparticles prepared by auto combustion method," *Materials Science in Semiconductor Processing*, vol. 29, pp. 372–379, 2015.

[21] S. Jaballah, M. Benamara, H. Dahman et al., "Effect of Mg-doping ZnO nanoparticles on detection of low ethanol concentrations," *Materials Chemistry and Physics*, vol. 255, p. 123643, 2020.

[22] A. J. Kulandaisamy, J. R. Reddy, P. Srinivasan et al., "Room temperature ammonia sensing properties of ZnO thin films grown by spray pyrolysis: effect of Mg doping," *Journal of Alloys and Compounds*, vol. 688, pp. 422–429, 2016.

[23] H. Gao, L. Xie, P. Gong, and H. Wang, "Detection of ethanol using a tunable interband cascade laser at 3.345 μm," *Photonic Sensors*, vol. 8, no. 4, pp. 303–309, 2018.

[24] C. Sun, S. Rajasekhara, Y. Chen, and J. B. Goodenough, "Facile synthesis of monodisperse porous Co3O4 microspheres with superior ethanol sensing properties," *Chemical Communications*, vol. 47, no. 48, pp. 12852–12854, 2011.

[25] T. Arakawa, K. Iitani, T. Sato, K. Toma, and K. Mitsubayashi, "Ethanol vapor imaging system "Sniffer camera" for evaluation of alcohol metabolism from breath and palm skin gas," *Procedia Engineering*, vol. 168, pp. 522–528, 2016.

[26] J. Liu, T. Wang, B. Wang et al., "Highly sensitive and low detection limit of ethanol gas sensor based on hollow ZnO/SnO2 spheres composite material," *Sensors and Actuators B: Chemical*, vol. 245, pp. 551–559, 2017.

[27] S. Sau, S. Chakraborty, T. Das, and M. Pal, "Ethanol sensing properties of nanocrystalline α-MoO3," *Frontiers in Materials*, vol. 6, p. 285, 2019.

[28] K. A. Alim, V. A. Fonoberov, M. Shamsa, and A. A. Balandin, "Micro-Raman investigation of optical phonons in ZnO nanocrystals," *Journal of Applied Physics*, vol. 97, no. 12, p. 124313, 2005.

[29] A. Usha and J. Christy, "Characterization, thermal effect on optical band gap energy and photoluminescence in wurtzite ZnO: Er nanocrystallites," *Materials today Proceedings*, vol. 3, no. 2, pp. 145–151, 2016.

[30] D. Kim, A. Hussain, H.-L. Lee, Y.-J. Moon, J. Y. Hwang, and S.-J. Moon, "Stepwise current increment sintering of silver nanoparticle structures," *Crystals*, vol. 11, no. 10, p. 1264, 2021.

[31] L. Umaralikhan and M. J. M. Jaffar, "Green synthesis of ZnO and Mg doped ZnO nanoparticles, and its optical properties," *Journal of Materials Science: Materials in Electronics*, vol. 28, no. 11, pp. 7677–7685, 2017.

[32] L. Kang, M. Zhang, and Z.-H. Liu, "IR spectra of manganese oxides with either layered or tunnel structures," *Spectrochimica Acta Part A Molecular and Biomolecular Spectroscopy*, vol. 67, no. 3-4, pp. 864–869, 2007.

[33] G. Yu, L. Yue, S. G. Liu, B. B. Huang, and X. Y. Zhang, "Hydrothermal preparation and photocatalytic activity of mesoporous $Au–TiO_2$ nanocomposite microspheres," *Journal of Colloid and Interface Science*, vol. 334, no. 1, pp. 58–64, 2009.

[34] G. H. Ning, X.-P. Zhao, and J. Li, "Structure and optical properties of $Mg_xZn_{1-x}O$ nanoparticles prepared by sol-gel method," *Optical Materials*, vol. 27, no. 1, pp. 1–5, 2004.

[35] J. Yang, Y. Wang, J. Kong, M. Yu, and H. Jin, "Synthesis of Mg-doped hierarchical ZnO nanostructures via hydrothermal method and their optical properties," *Journal of Alloys and Compounds*, vol. 657, pp. 261–267, 2016.

[36] H. R. Ghorbani, F. ParsaMehr, H. Pazoki, and B. M. Rahmani, "Synthesis of ZnO nanoparticles by precipitation method," *Oriental Journal of Chemistry*, vol. 31, no. 2, pp. 1219–1221, 2015.

[37] Q. He, C. Zhong, and J. W. Wu, "Magnetic iron oxide nanoparticles: synthesis and surface functionalization strategies," *Nanoscale Research Letters*, vol. 3, pp. 397–415, 2008.

[38] S. Jaballah, Y. Alaskar, I. AlShunaifi et al., "Effect of Al and Mg doping on reducing gases detection of ZnO nanoparticles," *Chemosensors*, vol. 9, no. 11, p. 300, 2021.

[39] E. Vinoth, S. Gowrishankar, and N. Gopalakrishnan, "Effect of Mg doping in the gas-sensing performance of RF-sputtered ZnO thin films," *Applied Physics A*, vol. 124, no. 6, p. 433, 2018.